Abstract: The extraordinary properties of second harmonic generation in negative-index metamaterials, where the Poynting vector and the wavevector have opposite directions are investigated. The "backward" phase-matching condition results in significant changes in the Manley-Rowe relations and in spatial distributions of the field intensities of the coupled waves.

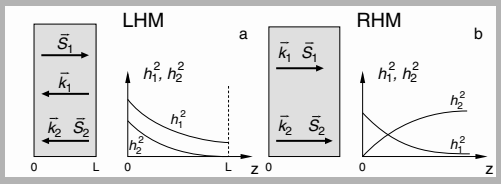

SHG in NIMs

Second harmonic generation in left-handed metamaterials

A.K. Popov, [1] *V.V. Slabko,* [2,3] *and V.M. Shalaev* [4,*]

[1] Department of Physics & Astronomy and Department of Chemistry, University of Wisconsin-Stevens Point, Stevens Point, WI 54481-3897, USA
[2] Krasnoyarsk State Technical University, Krasnoyarsk 660074, Russia
[3] Institute of Physics of the Russian Academy of Sciences, Krasnoyarsk 660036, Russia
[4] School of Electrical and Computer Engineering, Purdue University, West Lafayette, IN 47907-2035, USA

Received: 10 February 2006, Accepted: 13 February 2006
Published online: 21 February 2006

Key words: negative-index materials, metamaterials, negative-refraction, second harmonic generation

PACS: 78.67.-n, 42.65.-k, 78.20.Bh

1. Introduction

In the late 60s, V.G. Veselago suggested that the electromagnetic wave propagation in an isotropic medium with simultaneously negative dielectric permittivity ϵ and magnetic permeability μ would exhibit very unusual properties [1,2]. Specifically, the simultaneously negative dielectric permittivity, $\epsilon < 0$, and magnetic permeability, $\mu < 0$, lead to a negative refraction index, with the left-handed triplet of the electrical field, magnetic field and the wavevector. The energy-flow (Poynting vector) in this case is counter-directed with respect to the wavevector. It is rather counter-intuitive and in a sharp contrast with normal, positive-index materials (PIMs) [also referred to as right-handed materials (RHMs)]. The negative-index materials (NIMs) [also referred to as left-handed materials (LHMs)] do not exist naturally. It was also generally accepted in the physical optics that the magnetization at optical frequencies is negligible and, hence, didn't not play any essential role [3]. In accordance with this, the magnetic permeability μ was normally set to be equal to one in the basic Maxwell's equations, describing the linear and nonlinear optical processes [4].

Metamaterials, i.e., artificially designed and engineered materials, may have properties unattainable in nature, including a negative refractive index. Initially, metamaterials with a magnetic response and a negative refractive index were fabriacted for the microwave and terahertz frequency ranges [5,6]. The optical frequency range imposes increasing difficulties and challenges for metamaterials. The promising approaches for developing negative-index materials in the optical range were proposed in [7–9] and experimentally realized in 2005 [10,11]. A negative magnetic permeability in the optical range, which is a precursor for a negative refraction, has been also demonstrated recently in [12–14]. In parallel with progress for metal-dielectric metamaterials, experimental demonstrations of negative refraction in the near IR range have been made in a GaAs-based photonic crystals [15] and in Si-Polyimide photonic crystals [16].

The main emphasis in the studies of NIMs has been placed so far on linear optical effects. Recently it has

* Corresponding author: e-mail: shalaev@ecn.purdue.edu

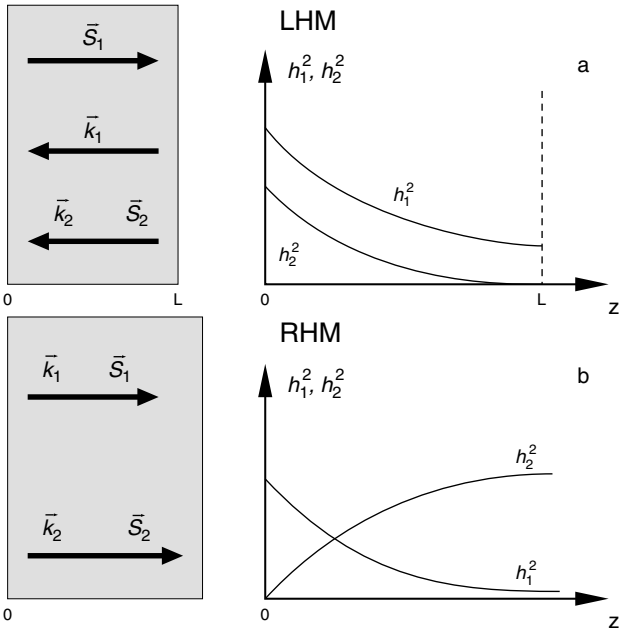

Figure 1 The difference in the phase-matching geometry and in the intensity-distribution for the fundamental and the second harmonic waves, h_1^2 and h_2^2, between a slab of the left-handed metamaterial – (a), and a right-handed material – (b)

been shown that NIMs including structural elements with non-symmetric current-voltage characteristics can possess a nonlinear magnetic response at optical frequencies [17–19] and thus combine unprecedented linear and nonlinear electromagnetic features. Important properties of second harmonic generation (SHG) in NIMs in the constant-pump approximation were discussed in [20] for semi-infinite materials and in [21] for a slab of a finite thickness. The propagation of microwave radiation in nonlinear transmission lines, which are the one-dimensional analog of NIMs, was investigated in [22]. The possibility of the exact phase-matching for waves with counter-propagating energy-flows has been shown in [23] for the case when the fundamental wave falls in the negative-index frequency domain and the SH wave lies in the positive-index domain. The possibility of the existence of multistable nonlinear effects in SHG was also predicted in [23]. This opens new avenues in optics and promise a great variety of unprecedented applications for optics and especially nonlinear optics. Absorption is one of the most challenging problems that needs to be addressed for practical applications of NIMs. A transfer of the near-field image into second-harmoniv (SH) frequency domain, where absorption is typically much less, was proposed in [20,21] as a possible means to overcome dissipative losses and thus enable the superlens.

In this paper, we demonstrate counter-intuitive effects and unusual characteristics in the spatial distribution of the energy exchange between the fundamental and second-harmonic backward waves beyond the constant-pump approximation. Both semi-infinite and finite-length NIM slabs are considered and compared with each other and with ordinary PIMs. In order to focus on the basic features of the process, our analysis is based on the solution to equations for the slowly varying amplitudes of the coupled backward fundamental and second-harmonic waves propagating in lossless NIMs. The Manley-Rowe relations for NIMs are analyzed and they are shown to be strikingly different from those in PIMs. The feasibility of a nonlinear-optical mirror converting 100% of the incident radiation into a reflected SH is shown for the case of a loss-free NIM.

The paper is organized as follows. The waves' "backward" features, which are inherent to NIMs, are discussed in Sec. 2. The basic equations for the negative-index fundamental and positive-index SH waves are derived and the relevant Manley-Rowe relations are discussed and compared with those in PIMs in Sec. 3. The unusual spatial distributions of the field intensities for SHG in a NIM slab of a finite-thickness are described in Sec. 4. The properties of a nonlinear-optical mirror with a semi-infinite thickness, converting an incident fundamental beam into a reflected SH beam are analyzed in Sec. 5. Finally, a summary for the obtained results concludes the paper.

2. Wavevectors and Poynting vectors for the fundamental and second harmonic waves in a double-domain metamaterial

We consider a loss-free material, which is left-handed at the fundamental frequency ω_1 ($\epsilon_1 < 0$, $\mu_1 < 0$), whereas it is right-handed at the SH frequency $\omega_2 = 2\omega_1$ ($\epsilon_2 > 0$, $\mu_2 > 0$). The relations between the vectors of the electrical, $\mathbf{E}$, and magnetic, $\mathbf{H}$, field components and the wavevector $\mathbf{k}$ for an electromagnetic wave

$$\mathbf{E}(\mathbf{r},t) = \mathbf{E}_0(\mathbf{r}) \exp[-i(\omega t - \mathbf{k}\cdot\mathbf{r})] + c.c.\,, \tag{1}$$

$$\mathbf{H}(\mathbf{r},t) = \mathbf{H}_0(\mathbf{r}) \exp[-i(\omega t - \mathbf{k}\cdot\mathbf{r})] + c.c.\,, \tag{2}$$

traveling in a loss-free medium with the dielectric permittivity ϵ and magnetic permeability μ are given by the equations

$$\mathbf{k}\times\mathbf{E} = \frac{\omega}{c}\,\mu\mathbf{H}\,, \quad \mathbf{k}\times\mathbf{H} = -\frac{\omega}{c}\,\epsilon\mathbf{E}\,, \tag{3}$$

$$\sqrt{\epsilon}E(\mathbf{r},t) = -\sqrt{\mu}H(\mathbf{r},t)\,, \tag{4}$$

which follow from the Maxwell's equations. Eqs. (3) show that the vector triplet $\mathbf{E}$, $\mathbf{H}$ and $\mathbf{k}$ forms a right-handed system for the SH wave and a left-handed system for the fundamental beam. Simultaneously negative $\epsilon < 0$ and $\mu < 0$ result in a negative refractive index $n = -\sqrt{\mu\epsilon}$. As seen from Eqs. (1) and (2), the phase velocity $\mathbf{v}_{ph}$ is co-directed with $\mathbf{k}$ and is given by $\mathbf{v}_{ph} = (\mathbf{k}/k)(\omega/k) = (\mathbf{k}/k)(c/|n|)$, where $k^2 = n^2(\omega/c)^2$. In contrast, the direction of the energy flow (Poynting vector) $\mathbf{S}$ with respect to $\mathbf{k}$ depends on the signs of ϵ and μ:

$$\mathbf{S}(\mathbf{r},t) = \frac{c}{4\pi}\,[\mathbf{E}\times\mathbf{H}] = \tag{5}$$

$$= \frac{c^2}{4\pi\omega\epsilon}\,[\mathbf{H}\times\mathbf{k}\times\mathbf{H}] = \frac{c^2\mathbf{k}}{4\pi\omega\epsilon}H^2 = \frac{c^2\mathbf{k}}{4\pi\omega\mu}E^2\,.$$

As mentioned, we assume here that all indices of ϵ, μ, and n are real numbers. Thus, the energy-flow $\mathbf{S}_1$ at ω_1 is directed opposite to $\mathbf{k}_1$, whereas $\mathbf{S}_2$ is co-directed with $\mathbf{k}_2$.

3. Basic equations and the Manley-Rowe relations for SHG process in NIMs and PIMs

3.1. Basic equations

We assume that an incident flow of fundamental radiation $\mathbf{S}_1$ at ω_1 propagates along the z-axis, which is normal to the surface of a metamaterial. According to (5), the phase of the wave at ω_1 travels in the reverse direction inside the NIM (Fig. 1a). Because of the phase-matching requirement, the generated SH radiation also travels backward with energy flow in the same backward direction. This is in contrast with the standard coupling geometry in a PIM (Fig. 1b).

Following the method of [23], we assume that a nonlinear response is primarily associated with the magnetic component of the waves. Then the equations for the coupled fields inside a NIM in the approximation of slow-varying amplitudes acquire the form:

$$\frac{dA_2}{dz} = i\sigma_2 A_1^2\exp(-i\Delta kz)\,, \tag{6}$$

$$\frac{dA_1}{dz} = i\sigma_1 A_2 A_1^*\exp(i\Delta kz)\,. \tag{7}$$

Here, $\Delta k = k_2 - 2k_1$; $\sigma_1 = (\epsilon_1\omega_1^2/k_1c^2)8\pi\chi^{(2)}$, $\sigma_2 = (\epsilon_2\omega_2^2/k_2c^2)4\pi\chi^{(2)}$; $\chi^{(2)}$ is the effective nonlinear susceptibility; A_2 and A_1 are the slowly varying amplitudes of the waves with the phases traveling against the z-axis,

$$H_j(z,t) = A_j\exp[-i(\omega_j t + k_j z)] + c.c.\,, \tag{8}$$

$j = \{1,2\}$; $\omega_2 = 2\omega_1$; and $k_{1,2} > 0$ are the moduli of the wavevectors directed against the z-axis. We note that according to Eq. (4) the corresponding equations for the electric components can be written in a similar form, with ϵ_j substituted by μ_j and vice versa. The factors μ_j were usually assumed to be equal to one in similar equations for PIMs. However, this assumption does not hold for the case of NIMs, and this fact dramatically changes many conventional electromagnetic relations.

3.2. Manley-Rowe relations

The Manley-Rowe relations [24] for the field intensities and for the energy flows follow from Eqs. (5-7):

$$\frac{k_1}{\epsilon_1}\frac{d|A_1|^2}{dz} + \frac{k_2}{2\epsilon_2}\frac{d|A_2|^2}{dz} = 0\,, \tag{9}$$

$$\frac{d|S_1|}{dz} - \frac{d|S_2|}{dz} = 0\,.$$

The latter equation accounts for the difference in the signs of ϵ_1 and ϵ_2, which brings radical changes to the spatial dependence of the field intensities discussed below.

In order to outline the basic difference between the SHG process in NIMs and PIMs, we assume in our further consideration that the phase matching condition $k_2 = 2k_1$ is fulfilled. The spatially-invariant form of the Manley-Rowe relations follows from Eq. (9):

$$\frac{|A_1|^2}{\epsilon_1} + \frac{|A_2|^2}{\epsilon_2} = C\,, \tag{10}$$

where C is an integration constant. With $\epsilon_1 = -\epsilon_2$ Eq. (10) predicts that the *difference* between the squared amplitudes remains constant through the sample

$$|A_1|^2 - |A_2|^2 = C\,, \tag{11}$$

as schematically depicted in Fig. 1a. This is in striking difference with the requirement that the *sum* of the squared amplitudes is constant in the analogous case in a PIM, as schematically shown in Fig. 1b.

We introduce now the real phases and amplitudes as $A_{1,2} = h_{1,2}\exp(i\phi_{1,2})$. Then the equations for the real amplitudes and phases, which follow from Eqs. (6) and (7), show that if any of the fields becomes zero at any point, the integral (10) corresponds to the solution with the constant phase difference $2\phi_1 - \phi_2 = \pi/2$ over the entire sample.

3.3. SHG in PIMs

The equations for the slowly-varying amplitudes corresponding to the ordinary coupling scheme in a PIM, shown in Fig. 1b, are readily obtained from Eqs. (6–8) by changing the signs of k_1 and k_2. This does not change the integral (10); more importantly, the relation between ϵ_1 and ϵ_2 required by the phase matching now changes to $\epsilon_1 = \epsilon_2$, where both constants are positive. The phase difference remains the same. Because of the boundary conditions $h_1(0) = h_{10}$ and $h_2(0) = h_{20} = 0$, the integration constant becomes $C = h_{10}^2$. Thus, the equations for the real amplitudes in the case of a PIM acquire the form:

$$h_1(z) = \sqrt{h_{10}^2 - h_2(z)^2}\,, \tag{12}$$

$$\frac{dh_2}{dz} = \kappa\left[h_{10}^2 - h_2(z)^2\right]\,, \tag{13}$$

with the known solution

$$h_2(z) = h_{10}\tanh\left(\frac{z}{z_0}\right)\,, \tag{14}$$

$$h_1(z) = \frac{h_{10}}{\cosh\left(\frac{z}{z_0}\right)}\,, \quad z_0 = \frac{1}{\kappa h_{10}}\,. \tag{15}$$

Here, $\kappa = (\epsilon_2\omega_2^2/k_2c^2)4\pi\chi^{(2)}_{eff}$. *The solution has the same form for an arbitrary slab thickness* with decreasing fundamental and increasing SH squared amplitudes along z-axis, as shown schematically in Fig. 1b.

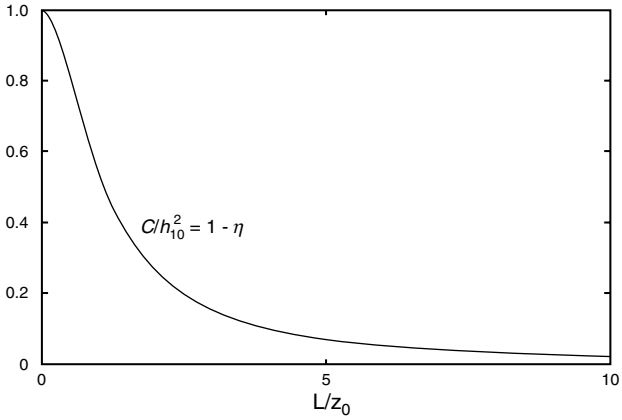

Figure 2 The normalized integration constant C/h_{10}^2 and the energy conversion efficiency η vs the normalized length of a NIM slab

4. SHG in a NIM slab

Now consider phase-matched SHG in a lossless NIM slab of a finite length L. Eqs. (6) and (11) take the form:

$$h_1(z)^2 = C + h_2(z)^2\,, \tag{16}$$

$$\frac{dh_2}{dz} = -\kappa\left[C + h_2(z)^2\right]\,. \tag{17}$$

Taking into account the *different boundary conditions in a NIM as compared to a PIM*, $h_1(0) = h_{10}$ and $h_2(L) = 0$, the solution to these equations is as follows

$$h_2 = \sqrt{C}\tan\left[\sqrt{C}\kappa(L-z)\right]\,, \tag{18}$$

$$h_1 = \frac{\sqrt{C}}{\cos\left[\sqrt{C}\kappa(L-z)\right]}\,, \tag{19}$$

where the integration parameter C *depends on the slab thickness* L and on the amplitude of the incident fundamental radiation as

$$\sqrt{C}\kappa L = \arccos\left(\frac{\sqrt{C}}{h_{10}}\right)\,. \tag{20}$$

Thus, *the spatially invariant field intensity difference between the fundamental and SH waves in NIMs depends on the slab thickness, which is in strict contrast with the case in PIMs.* As seen from Eq. (16), the integration parameter $C = h_1(z)^2 - h_2(z)^2$ now represents the deviation of the conversion efficiency $\eta = h_{20}^2/h_{10}^2$ from unity: $(C/h_{10}^2) = 1 - \eta$. Fig. 2 shows the dependence of this parameter on the conversion length $z_0 = (\kappa h_{10})^{-1}$.

The figure shows that for the conversion length of 2.5, the NIM slab, which acts as nonlinear mirror, provides about 80% conversion of the fundamental beam into a reflected SH wave. Fig. 3 depicts the field distribution along the slab. One can see from the figure that with an increase

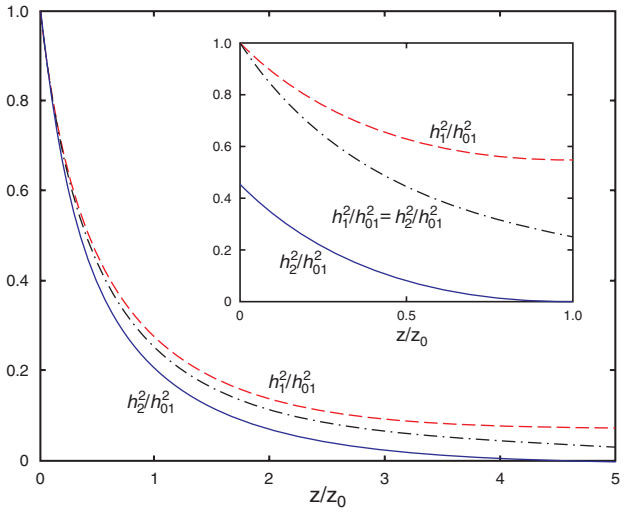

Figure 3 (online color at www.lphys.org) The squared amplitudes for the fundamental wave (the dashed line) and SHG (the solid line) in a lossless NIM slab of a finite length. Inset: the slab has a length equal to one conversion length. Main plot: the slab has a length equal to five conversion lengths. The dash-dot lines show the energy-conversion for a semi-infinite NIM

in slab length (or intensity of the fundamental wave), the gap between the two plots decreases while the conversion efficiency increases (comparing the main plot and the inset).

5. SHG in a semi-infinite NIM

Now we consider the case of a semi-infinite NIM at $z > 0$. Since both waves disappear at $z \to \infty$ due to the entire conversion of the fundamental beam into SH, $C = 0$. Then Eqs. (16) and (17) for the amplitudes take the simple form

$$h_2(z) = h_1(z)\,, \tag{21}$$

$$\frac{dh_2}{dz} = -\kappa h_2^2\,. \tag{22}$$

Eq. (21) indicates 100% conversion of the incident fundamental wave into the reflected second harmonic at $z = 0$ in a lossless semi-infinite medium provided that the phase matching condition $\Delta k = 0$ is fulfilled. The integration of (22) with the boundary condition $h_1(0) = h_{10}$ yields

$$h_2(z) = \frac{h_{10}}{\left(\frac{z}{z_0}\right) + 1}\,, \quad z_0 = \frac{1}{\kappa h_{10}}\,. \tag{23}$$

Eq. (23) describes a *concurrent decrease of both waves of equal amplitudes along the z-axis;* this is shown by the dash-dot plots in Fig. 3. For $z \gg z_0$, the dependence is inversely proportional to z. These *spatial dependencies, shown in Fig. 3, are in strict contrast with those for the conventional process of SHG in a PIM*, which are known from various textbooks (compare, for example, with Fig. 1b).

6. Conclusion

We have studied the unusual properties of second-harmonic generation (SHG) in metamaterials that have a negative refractive index for the fundamental wave and a positive index for its second harmonic (SH). The possibility of a left-handed nonlinear-optical mirror, which converts the incoming radiation into a reflected beam at the doubled frequency with efficiency that can approach 100% for lossless and phase-matched medium is considered. The most striking differences in the nonlinear propagation and the spatial dependence of the energy-conversion process for SHG in NIMs, as compared to PIMs, can be summarized as follows. In NIMs, the intensities of the fundamental and SH waves both decrease along the medium. Such unusual dependence and the apparent contradiction with the ordinary Manley-Rowe relations are explained by the fact that the energy flows for the fundamental and SH waves are counter-directed, whereas their wavevectors are co-directed. Another interesting characteristic of SHG in NIMs is that the energy conversion at any point within a NIM slab depends on the total thickness of the slab. This is because SHG in a NIM is determined by the boundary condition for SH at the rear interface rather than at the front interface of the slab.

The backward energy flow for one of the coupled waves (whereas the wavevectors of both coupled waves are co-directed) is inherent for phase-matching in NIMs and it makes this process different from SHG in PIMs. This is also different from various processes in RHMs based on distributed gratings and feedback. In NIMs, each spatial point serves as a source for the generated wave in the reflected direction, whereas the phase velocities of the coupled waves are co-directed. We note here that the important advantages of interaction schemes involving counter-directed Poynting vectors in the process of optical parametric amplification in ordinary RHMs were discussed in early papers [25]. However, in RHMs such schemes impose severe limitations on the frequencies of the coupled waves because of the requirement that one of the waves has to be in the far-infrared range. The process investigated herein is free from the PIM limitations.

Acknowledgements The authors are grateful to S.A. Myslivets for help with numerical analysis. This work was supported in part by NSF-NIRT award ECS-0210445, by ARO grant W911NF-04-1-0350, Russian grant DSP 2.1.1.1814, and by DARPA under grant No. MDA 972-03-1-0020.

References

[1] V.G. Veselago, Sov. Phys. Solid State **8**, 2854 (1967).
[2] V.G. Veselago, Usp. Fiz. Nauk **92**, 517 (1967) [Sov. Phys. Usp. 10, 509 (1968)].
[3] L.D. Landau and E.L. Lifshits, Electrodinamics of Continuous Media, 2nd. ed. (Pergamon Press, New York, 1960), Ch. 9.
[4] R.W. Boyd, Nonlinear Optics, 2nd ed. (Academic Press, New York, 2003).
[5] D.R. Smith, W. Padilla, D.C. Vier, S.C. Nemat-Nasser, and S. Shults, Phys. Rev. Lett. **84**, 4184 (2000).
[6] D.R. Smith, J.B. Pendry, and M.C.K. Wiltshire, Science **305**, 788 (2004).
[7] M. Notomi, Phys. Rev. B **62**, 10696 (2000).
[8] V.A. Podolskiy, A.K. Sarychev, and V.M. Shalaev, J. Nonlin. Opt. Phys. Mater. **11**, 65 (2002).
[9] V.A. Podolskiy, A.K. Sarychev, and V.M. Shalaev, Opt. Express **11**, 735 (2003).
[10] V.M. Shalaev, W. Cai, U. Chettiar, H.-K. Yuan, A.K. Sarychev, V.P. Drachev, and A.V. Kildishev, Opt. Lett. **30**, 3356 (2005); first reported in arXiv: physics/0504091 (2005); V.P. Drachev, W. Cai, U. Chettiar, H.-K. Yuan, A.K. Sarychev, A.V. Kildishev, G. Klimeck, and V.M. Shalaev, Laser Phys. Lett. **3**, 49 (2006).
[11] S. Zhang, W. Fan, N.C. Panoiu, K.J. Malloy, R.M. Osgood, and S.R.J. Brueck, Phys. Rev. Lett. 95, 137404 (2005); arXiv: physics/0504208 (2005).
[12] S. Linden, C. Enkrich, M. Wegener, J. Zhou, T. Koschny, and C.M. Soukoulis, Science **306**, 1351 (2004).
[13] Z. Zhang, W. Fan, B.K. Minhas, A. Frauenglass, K.J. Malloy, and S.R.J. Brueck, Phys. Rev. Lett. **94**, 037402 (2005).
[14] A.N. Grigorenko, A.K. Geim, N.F. Gleeson, Y. Zhang, A.A. Firsov, I.Y. Khrushchev, and J. Petrovic, Nature **438**, 335 (2005).
[15] A. Berrier, M. Mulot, M. Swillo, M. Qiu, L. Thylén, A. Talneau, and S. Anand, Phys. Rev. Lett. **93**, 73902 (2004).
[16] E. Schonbrun, M. Tinker, W. Park, and J.-B. Lee, IEEE Photon. Tech. Lett. **17**, 1196 (2005).
[17] M. Lapine, M. Gorkunov, and K.H. Ringhofer, Phys. Rev. E **67**, 065601 (2003).
[18] A.A. Zharov, I.V. Shadrivov, and Yu.S. Kivshar, Phys. Rev. Lett. **91**, 037401 (2003).
[19] M. Lapine and M. Gorkunov, Phys. Rev. E **70**, 66601 (2004).
[20] V.M. Agranovich, Y.R. Shen, R.H. Baughman, and A.A. Zakhidov, Phys. Rev. B **69**, 165112 (2004).
[21] A.A. Zharov, N.A. Zharova, Il.V. Shadrivov and Yu.S. Kivshar, Appl. Phys. Lett. **87**, 091104 (2005).
[22] A.B. Kozyrev, H. Kim, A. Karbassi, and D.W. van der Weide, Appl. Phys. Lett. **87**, 121109 (2005).
[23] I.V. Shadrivov, A.A. Zharov, and Yu.S. Kivshar, arXiv: physics/0506092 (2005).
[24] J.M. Manley and H.E. Rowe, Proc. IRE **47**, 2115 (1959).
[25] S.E. Harris, Appl. Phys. Lett. **9**, 114 (1966); K.I. Volyak and A.S. Gorshkov, Radiotekhnika i Elektronika (Radiotechnics and Electronics) **18**, 2075 (1973), in Russian; A. Yariv, Quantum Electronics, 2d ed. (Wiley, New York, 1975), Ch. 18.